ACS OMEGA

Open Access

http://pubs.acs.org/journal/acsodf

Article

Preparation of Temperature-Sensitive Molecularly Imprinted Cryogel for Specific Recognition of Proteins

Dandan Cheng,* Yahong Chen, Yalan Feng, Yijun Zeng, and Zhao Zhao*

Cite This: *ACS Omega* 2025, 10, 11312−11324

Read Online

ACCESS | Metrics & More | Article Recommendations | Supporting Information

ABSTRACT: In order to maintain the stability of the structure of protein molecules and improve the recognition during the separation process, molecular imprinting technology is combined with freeze polymerization to synthesize molecular imprinting cryogels (MICs). This study uses bovine serum albumin (BSA) as a template protein, low critical cosolubility temperature (LCST)-type ionic liquids as temperature-sensitive functional monomers, imidazole ionic liquids, and acrylamides as auxiliary functional monomers to prepare MICs with specific recognition, temperature sensitivity, interpenetrating macroporous structure, and large specific surface area. The MICs prepared at freezing temperature have uniform macroporous structures and good mechanical properties, which is conducive to the improvement of the mass transfer and adsorption capacities. Due to the advantages, the MIC reaches the adsorption equilibrium within 125 min with a saturated adsorption capacity of 741.5 mg g^{-1} and an imprinting factor of 1.65. Their static and dynamic adsorption behaviors are more in line with the Langmuir model and the quasi-secondary kinetic model, respectively. In addition, the MIC has obvious temperature sensitivity, and the maximum adsorption amount is reached at 37 °C. The separation factor (relative to cytochrome *c*, bovine blood hemoglobin, and lysozyme) of the MICs for BSA is up to 1.39. Repeatability experiments reveal that the adsorption capacity of molecularly imprinted cryogels is retained at 87% after five adsorption−desorption cycles, indicating excellent recyclability and potential for practical application.

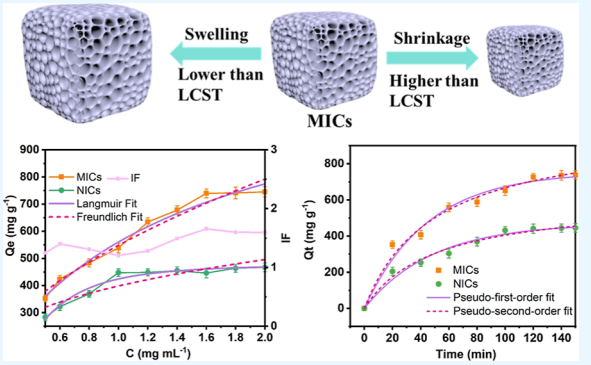

1. INTRODUCTION

Protein molecular imprinting techniques can specifically separate proteins, but the uniqueness of proteins hinders their development.[1−3] The large size of proteins increases the mass transfer resistance of the imprinted polymer during adsorption.[4] Besides, the complex structure and flexible conformation of proteins can cause mis-imprinting and reduce the accuracy of imprinting, resulting in poor specificity and low selectivity of the protein molecular imprinted polymers.[5] In addition, proteins can only exist stably in the aqueous environment, so it is necessary to select functional monomers that can produce multiple weak interactions with proteins in the aqueous phase to improve the specific recognition ability of the imprinted polymers.[2,6−8]

Cryogel is prepared by polymerization of monomers below the freezing point of the system.[9,10] Water is usually used as a solvent and pore-forming agent to form interpenetrating macroporous polymers through the formation and removal of ice crystals during the polymerization.[11−13] As the cryogel material has the advantages of good biocompatibility, mechanical stability, and low preparation cost, a new type of molecularly imprinted material, molecular imprinting cryogel (MIC), can be obtained by combining the material.[14,15] It is a new strategy to separate and purify proteins by combining the conformational predetermination and specific recognition of molecular imprinting technology with the porous structure and high throughput of cryogel.[16−19] Compared with traditional protein-imprinted methods such as surface-imprinted and antigen-determining cluster-imprinted, MICs have a more stable protein structure in the aqueous phase system.[20−22] Kartal and Denizli used functional monomers to prepare poly(2-hydroxyethyl methyl methacrylate-*n*-methylacrylyl-L-tryptophan methyl ester) cryogel beads with cholesterol-selective binding sites for improving the removal efficiency of cholesterol from milk.[16] MICs prepared using cholesterol as a template (CHO-MICs) obtain a larger surface area and selectivity than nonimprinted cryogels (NICs), so the selective adsorption capacity of CHO-MICs is nearly 5 times that of NICs in the presence of competitive analogues. The prepared MIC material has high toughness, interpenetrating large pores and a large specific surface area, which solves the problems of mis-imprinting, elution difficulty, and low recognition

Received: December 9, 2024
Revised: February 4, 2025
Accepted: February 19, 2025
Published: March 11, 2025

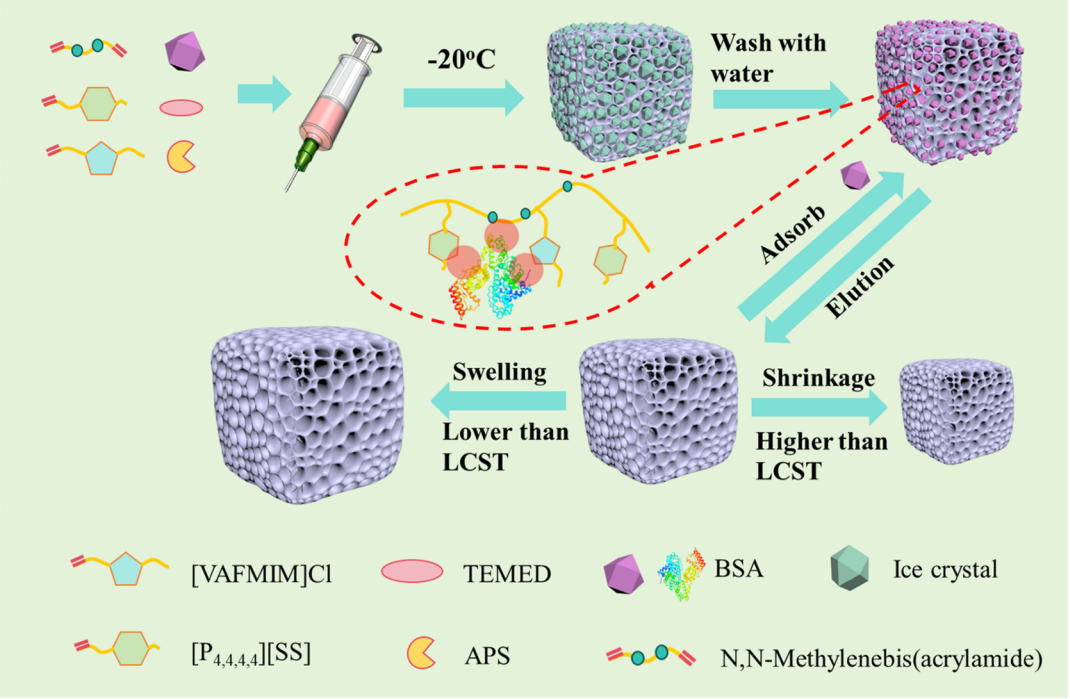

Figure 1. Preparation route of MICs.

efficiency caused by the flexible and changeable protein structure and high mass transfer resistance in protein molecular imprinting.[22−24]

Introducing temperature-sensitive monomers into MICs, the volume of the prepared MICs shows expansion or contraction with temperature changes.[25−27] For heat-shrinkable temperature-sensitive MICs, the MIC material is in an expanded state when the temperature is lower than the lowest critical phase transition temperature (LCST), which is conducive to the imprinting and elution of the template protein molecules and reduces the mass-transfer resistance of the proteins in the adsorption process.[22,28] When the temperature is higher than LCST, the MIC material shrinks, which is conducive to the immobilization of proteins in the cryogel network without destroying the protein structure and improves the specific recognition of MIC materials.[29−32] Overall, the introduction of temperature-sensitive monomers into MICs improves the specific recognition performance of MICs for target proteins and also achieves the automatic binding or release of target proteins.[33−35]

In this study, we propose to use low critical cosolubility temperature (LCST)-type ionic liquids, which can exhibit hydration or hydrophobicity depending on the external temperature, as functional monomers for the preparation of MIC materials. It can improve the adsorption and specific recognition of MICs through multiple interactions, such as hydrophobicity, hydrogen bonding, electrostatic forces, and $\pi-\pi$ conjugation with the surface groups of protein molecules. LCST-type *p*-styrenesulfonic acid tetrabutylphosphine salt ionic liquids ([$P_{4,4,4,4}$][SS]) and 1-vinyl-3-carbamoylmethylimidazole chlorate ionic liquids ([VAFMIM]Cl) are synthesized. Due to the good water solubility, the functional groups in the anions and cations can produce multiple interactions with proteins, producing a large number of accurate binding sites for protein recognition. Acrylamide has also been used as a functional monomer to improve the force between the imprinted material and proteins through strong hydrogen bonding interactions with proteins. In addition, acrylamide enhances the mechanical properties of the MICs materials, which is helpful in achieving a stable performance of MICs during adsorption.

2. EXPERIMENT

2.1. Materials. Tetrabutylphosphonium bromide (98%, [$P_{4,4,4,4}$]Br), sodium *p*-styrenesulfonate (≥98%), acrylamide (99%), 2-chloroacetamide (≥98%), and 1-vinylimidazole (99%) are provided by Shanghai Macklin Biochemical Co., Ltd. Acetone (AR) is purchased from Guangdong Guanghua Technology Co., Ltd. Bovine serum albumin (≥96%, BSA), bovine blood hemoglobin (BHb), cytochrome *c* (95%, Cyt *c*), lysozyme (Lyz), *N*,*N*-methylenebis(acrylamide) (99%), *N*,*N*,*N*′,*N*′-tetramethylethylenediamine (TEMED, 99%), and ammonium persulfate (≥98%) are purchased from Shanghai Aladdin Biochemical Technology Co., Ltd.

2.2. Synthesis of Temperature-Sensitive Ionic Liquids [$P_{4,4,4,4}$][SS]. Equimolar tetrabutylphosphonium bromide ([$P_{4,4,4,4}$]Br) and sodium *p*-styrenesulfonate (Na[SS]) were added to a distillation flask containing 100 mL of ultrapure water, and the mixture was reacted at room temperature for 24 h. The water in the solution was removed by rotary evaporation to obtain a white oily liquid. It was then dissolved in 10 mL of ultrapure water and freeze-dried for 48 h to obtain the white solid *p*-styrenesulfonic acid tetrabutylphosphine salt ([$P_{4,4,4,4}$][SS]). The reaction equation is shown in Figure S1, and its structure was characterized by Fourier transform infrared spectroscopy (FTIR) and nuclear magnetic resonance hydrogen spectroscopy (^{1}H NMR), and the results are shown in Figures S2 and S3.

2.3. Synthesis of Imidazole Functional Monomers [VAFMIM]Cl. A solution was prepared by dissolving 10 g of 2-chloroacetamide into 200 mL of acetone, and 10.03 g of 1-vinylimidazole was added dropwise under a nitrogen

https://doi.org/10.1021/acsomega.4c11143
ACS Omega 2025, 10, 11312−11324

atmosphere. Then the reaction occurred according to the reaction equation in Figure S4 with stirring at 50 °C for 24 h. The white reaction product obtained by filtration was washed three times with acetone, dissolved in 10 mL of ultrapure water, and then freeze-dried for 48 h to obtain a white solid 1-vinyl-3-carbamoylmethylimidazole chloride ([VAFMIM]Cl). The structure of the product was characterized by Fourier transform infrared spectroscopy (FTIR) and nuclear magnetic resonance hydrogen spectroscopy (^{1}H NMR), and the results are shown in Figures S5 and S6.

2.4. Preparation of MICs. The preparation process of MICs is shown in Figure 1. 200 mg of BSA was dissolved into 3.0 mL of phosphate buffer (0.01 mol L^{-1}, pH = 7.4), and the functional monomers were added sequentially according to the ratio of the mole ratio of BSA/[$P_{4,4,4,4}$][SS]/[VAFMIM]Cl/acrylamide = 1:50:100:100. The mixture was stirred under a nitrogen atmosphere at 4 °C for 1 h. Then, *N*,*N*-methylenebis-(acrylamide) and ammonium persulfate (APS), which accounted for 10 wt % of the mass of the monomer and 20 wt % of the mass of the monomer respectively, were added and stirred for 30 min followed by the addition of 5 μL of *N*,*N*,*N*′,*N*′-tetramethylethylenediamine (TEMED). Finally, the above solution was transferred to a 2.5 mL syringe and reacted at −20 °C for 24 h to obtain a white columnar cryogel polymer. The above BSA-MICs polymer was washed with 100 mL of distilled water to remove the ice crystals and then washed with 0.5 mol L^{-1} sodium chloride solution to remove the BSA and unreacted functional monomers. The template protein (BSA) in the eluate was detected using a UV−visible spectrophotometer at 278 nm until the UV absorbance was lower than 0.1. After the elution was completed, the prepared temperature-sensitive MICs were washed several times with distilled water to remove the sodium chloride, and the BSA-MICs were obtained by freeze-drying for 36 h. Nonimprinted temperature-sensitive cryogels (NICs) were prepared in the same steps except that the template protein BSA was not added.

2.5. Effect of Functional Monomers on the Stability of BSA. The effect of functional monomers on the structural stability of BSA was investigated in the aqueous solution of BSA with a concentration of 1.1×10^{-6} mol L^{-1}. The mole ratios of BSA to the functional monomer were 1:0, 1:10, 1:20, 1:30, 1:50, 1:100, and 1:200, respectively. The adsorption was performed for 24 h under −20 °C, and then a series of circular dichroism (CD) spectroscopy and simultaneous fluorescence spectroscopy were obtained. Circular dichroism (CD) can be used to detect the stability of protein structure mainly because the changes in protein secondary structure can be sensitively reflected in the changes in the circular dichroism spectral curve. CD is a spectroscopic method to study the conformation of a protein by measuring the difference in absorbance of the protein to left- and right-handed circularly polarized light. This method takes advantage of the optically active properties of proteins, namely, that they contain chiral centers that are able to rotate the vibrational direction of plane-polarized light. Secondary structures of proteins, such as α-helices and β-folds, produce circular dichroic signals at specific wavelengths. By measurement of these signals, the conformation of the protein can be deduced. Fluorescence spectroscopy refers to the study of conformational changes of protein molecules by measuring the self-fluorescence of protein molecules or by introducing fluorescence probes to special parts of protein molecules and then measuring their fluorescence. When foreign substances are noncovalently bound to the nonpolar region of protein molecules, their fluorescence spectra will blue shift with the increase of the nonpolarity of the environment, and the fluorescence intensity will also increase, and vice versa. In a certain range, the fluorescence intensity has a linear relationship with the protein concentration. This property can be used to measure the change of polarity of the protein site bound by foreign substances, and the change of the protein structure can be further inferred according to the change of polarity. The effect of functional monomers on the secondary structure of BSA and the microenvironment of amino acid residues was analyzed to study the effect on the stability of proteins.

2.6. Effect of Temperature on the Adsorption Properties of MICs. A PBS (0.01 mol L^{-1}, pH = 7.4) solution of BSA at a concentration of 1.1×10^{-6} mol L^{-1} was configured and circular dichroism (CD) spectra were obtained at different temperatures (10, 20, 25, 30, 37, 40, 45, and 50 °C), respectively. 40 mL of 1.6 mg mL^{-1} BSA solution at different temperatures (10, 20, 25, 30, 37, 40, 45, and 50 °C) was adsorbed in 25 g of MICs and NICs for 2 h, respectively. The absorbance of BSA in the adsorbed solution was measured using a UV spectrophotometer at a wavelength of 278 nm, and the adsorption amount of BSA was calculated according to eqs 1 and 2, in which eq 1 was obtained according to the method described in the Supporting Information.

$$y = 0.6534x - 0.0078 \tag{1}$$

$$Q_e = \frac{(C_0 - C_e)V}{m} \tag{2}$$

where y is the value of absorbance, x is the concentration of BSA solution (mg·mL^{-1}). Q_e is the adsorption capacity (mg g^{-1}), and C_0 and C_e are the solution concentrations before and after adsorption (mg·mL^{-1}). m is the mass of the adsorbent used adsorbent (g). V is the volume of solution used for adsorption (mL).

2.7. Adsorption Performance of MICs on BSA. To characterize the adsorption properties of MICs on BSA, 25 mg of MICs or NICs was added to 40 mL of PBS (0.01 mol L^{-1}, pH = 7.4) solution with different concentrations of BSA for a specific time of adsorption at 25 °C and then centrifuged to obtain the supernatant. The absorbance of the supernatant was measured by a UV spectrophotometer at a wavelength of 278 nm, and the concentration of BSA in the supernatant and the saturated adsorption amount of BSA (Q_e) were calculated by eqs 1 and 2, respectively. The imprinting factor (IF) of MICs was calculated according to eq 3 and the adsorption isotherms of MICs were plotted. The specific recognition, competitive adsorption, and cyclic regeneration properties of the MICs were also conducted, and the details are shown in the Supporting Information. Besides, the selection factor (β) was calculated according to eq 4 to evaluate the selective adsorption performance of the adsorbent to the target protein in the presence of other proteins.

$$IF = \frac{Q_{MICs}}{Q_{NICs}} \tag{3}$$

$$\beta = \frac{IF_{BSA}}{IF_{com}} \tag{4}$$

https://doi.org/10.1021/acsomega.4c11143
ACS Omega 2025, 10, 11312−11324

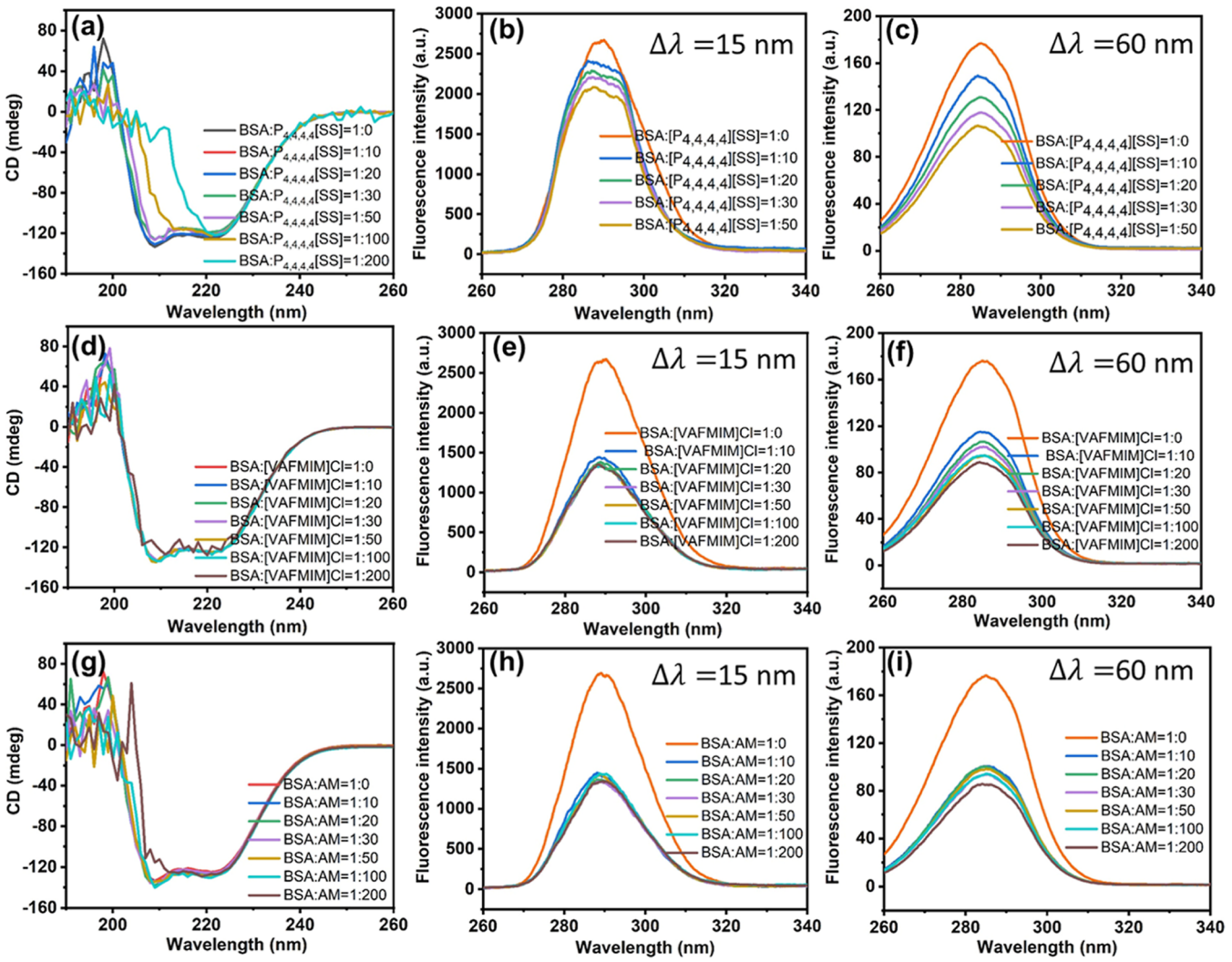

Figure 2. (a) CD spectra of BSA under the influence of $[P_{4,4,4,4}][SS]$; (b,c) Synchronous fluorescence spectra of BSA under the influence of $[P_{4,4,4,4}][SS]$; (d) CD spectra of BSA under the influence of [VAFMIM]Cl; (e,f) synchronous fluorescence spectra of BSA under the influence of [VAFMIM]Cl; (g) CD spectra of BSA under the influence of AM; and (h,i) synchronous fluorescence spectra of BSA under the influence of AM.

where Q_{MICs} and Q_{NICs} are the adsorption capacity of imprinted materials (MICs) and nonimprinted materials on BSA, respectively. IF_{BSA} and IF_{com} are the imprinting factors of the imprinting materials (MICs) for BSA and other proteins, respectively.

2.8. Characterization. The chemical structures of the MICs and NICs were characterized by a Fourier transform infrared spectrometer (TENSOR, Bruker) by using the KBr pellet method at ambient temperature. The mesoporous microstructure of the MICs and NICs was confirmed by scanning electron microscopy (SEM, Verios G4). A high-resolution spectrum of N 1s was recorded by X-ray photoelectron spectroscopy (XPS, Axis Ultra). Circular dichroism spectra were recorded on the spectrometer (CD, Chirascan V100) at a wavelength range of 180−260 nm and a scanning speed of 2.0 $nm \cdot s^{-1}$. Thermogravimetric analysis (TGA) was conducted on an analyzer (TGA-1, Mettler Toledo) with a heating rate of 10 °C min^{-1} within 25−800 °C. Differential scanning calorimetry (DSC) was conducted on an analyzer (DCS1, Mettler Toledo) with a scan rate of 10 °C min^{-1} within −50−100 °C.

3. RESULTS AND DISCUSSION

3.1. Effect of Functional Monomers on the Stability of Bovine Serum Albumin. Functional monomers in the aqueous phase that can produce multiple weak interactions with proteins can significantly improve the specific adsorption of the imprinted polymers.[36,37] However, many small molecule monomers can lead to the disruption of the protein structure under certain concentration and solvent conditions, which can reduce the accuracy and specificity of the imprinting process.[38,39] In this study, LCST-type ionic liquids ($[P_{4,4,4,4}][SS]$) were chosen as temperature-sensitive monomers for responding to changes in the external temperature. The imidazolium-based ionic liquid ([VAFMIM]Cl) was used as a cofunctional monomer for multiple weak interactions such as hydrogen bonding, electrostatic interaction, $\pi-\pi$ conjugation, and hydrophobic interaction with protein molecules.[8,40] The amide monomer (acrylamide, AM) is used to strengthen polymers in addition to providing hydrogen bonding for interaction with proteins.[41] However, the alteration of protein structure by these monomers affects the accurate formation of imprinting sites in the MICs, the imprinting efficiency, and the specificity of the MICs for the target protein.[42,43] Therefore, a

https://doi.org/10.1021/acsomega.4c11143
ACS Omega 2025, 10, 11312−11324

Table 1. Effect of Monomer on the α-Helix (%) of BSA at −20 °C

the molar ratio of BSA to monomer	1:0	1:10	1:20	1:30	1:50	1:100	1:200
$[P_{4,4,4,4}][SS]$	64.80%	64.5%	64.50%	64.10%	63.90%	50.80%	35.60%
[VAFMIM]Cl	64.80%	64.90%	65.60%	65.10%	64.00%	65.00%	55.20%
acrylamide	64.80%	65.90%	66.40%	68.70%	66.70%	69.60%	50.41%

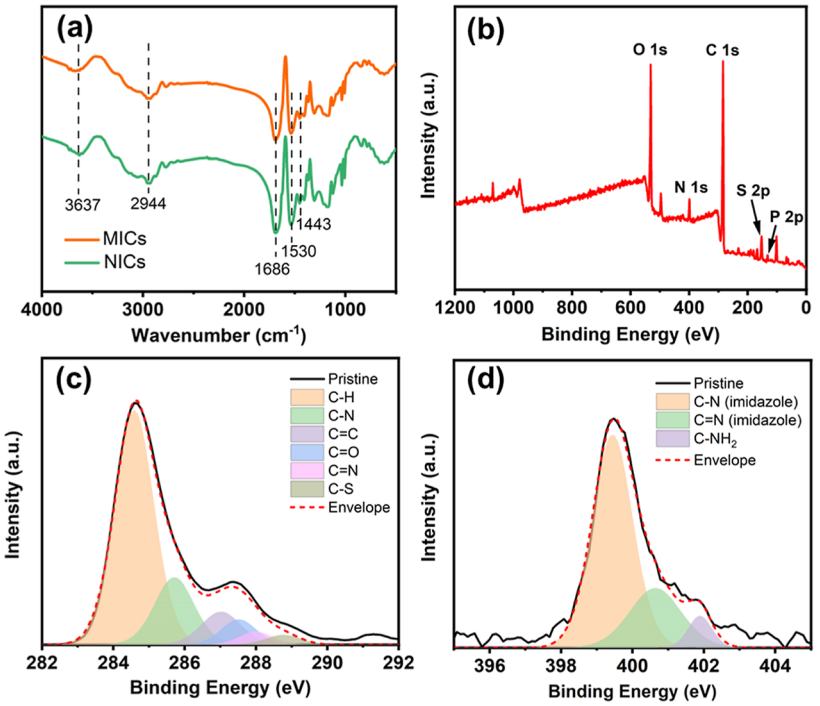

Figure 3. (a) FT-IR spectra of MICs and NICs; (b) XPS spectrum of MICs; high-resolution XPS spectra registered in the C 1s (c) and N 1s (d) regions.

systematic study of the effect of these monomers on the structure of BSA under freezing conditions needs to be carried out.

Figure 2a,d,g shows the CD spectra of BSA under the interaction of functional monomers at −20 °C for different molar ratios. As can be seen in Figure 2a,d,g, when the ratios of BSA to $[P_{4,4,4,4}][SS]$, [VAFMIM]Cl and AM are greater than 1:50, 1:100, and 1:100, respectively, the shapes of the two shoulder peaks at the characteristic peaks of 208 and 222 nm of BSA remained basically unchanged and the intensities are only slightly increased, which indicates that the secondary structure of BSA remains basically stable. The α-helix content in the secondary structure of the protein can be obtained after processing the information by the CD Spectra Deconvolution Software (CDNN) neural network fitting procedure, which can further determine the influence of functional monomers on the protein conformation under a freezing environment, and the results are shown in Table 1. Table 1 reflects more clearly that when the ratio of the molar amount of BSA to that of $[P_{4,4,4,4}][SS]$, [VAFMIM]Cl and AM is greater than 1:50, 1:100, and 1:100, respectively, the α-helix content of BSA is almost not altered, suggesting that the secondary structure of BSA remains stable. Therefore, when the ratio of the amount of BSA to $[P_{4,4,4,4}][SS]$, [VAFMIM]Cl, and AM is greater than 1:50, 1:100, and 1:100, respectively, the secondary structure of the protein BSA is well maintained, which is conducive to the formation of accurate imprinting sites.

Figure 2b,c,e,f,h,i shows the synchronous fluorescence spectra of BSA under the influence of different amounts of functional monomers at −20 °C with the fixed excitation wavelength and emission wavelength difference ($\Delta\lambda$) of 15 and 60 nm, respectively. As can be seen from Figure 2b,c,e,f,h,i, the fluorescence intensity of BSA decreases continuously with the increase of $[P_{4,4,4,4}][SS]$, [VAFMIM]Cl, and AM concentration at −20 °C when the excitation and emission wavelength difference ($\Delta\lambda$) is 15 and 60 nm. The decreased fluorescence intensity results from the fluorescence quenching of BSA, which is caused by the interaction between the monomer and BSA. For AM, the amino group of AM can form hydrogen bonds with the hydroxyl group and amino group in the protein molecule, increasing the interaction between the polyacrylamide-containing chain segment material and the protein molecule. The presence of acrylamide can increase the adsorption capacity of protein molecules, which can be verified by the effect of AM on the adsorption of MICs and NICs to BSA described in Supporting Information and Figure S8. Meanwhile, the position of the characteristic fluorescence spectral peaks of BSA does not shift significantly with the increasing monomer concentration, indicating that the structure of the protein is not significantly affected in this monomer concentration range. From the results of CD spectroscopy and synchronous fluorescence spectroscopy, it can be seen that the temperature-sensitive ionic liquids ($[P_{4,4,4,4}][SS]$), [VAFMIM]Cl, and acrylamide (AM) have less influence on the protein structure of BSA in the appropriate concentration range, which enables accurate imprinting of the protein molecule under freezing conditions.

https://doi.org/10.1021/acsomega.4c11143
ACS Omega 2025, 10, 11312−11324

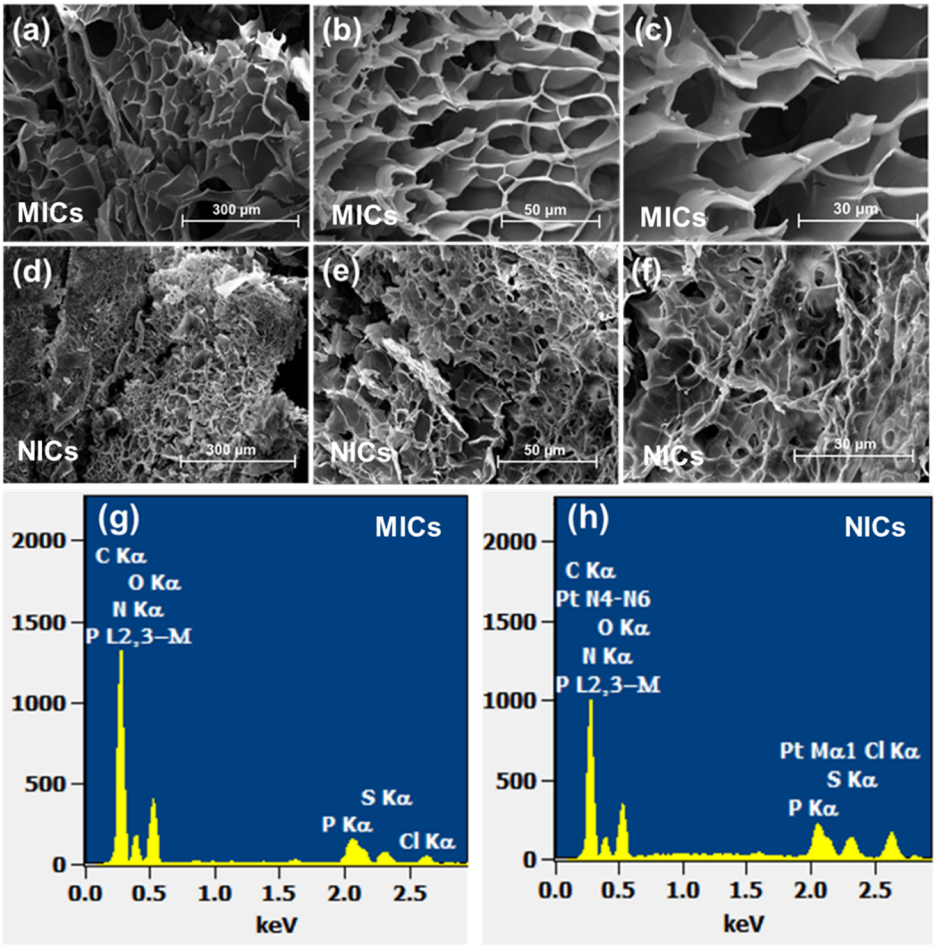

Figure 4. SEM images of MICs (a–c) and NICs (d–f); EDS images of MICs (g) and NICs (h).

3.2. Structure and Morphology of MICs. The structure of the synthesized MICs was characterized using Fourier transform infrared spectroscopy (FTIR) and X-ray photoelectron spectroscopy (XPS), and the results are shown in Figure 3. Figure 3a shows that the absorption peaks near 3457 cm^{-1} are the characteristic stretching vibration absorption peaks of $-NH_2$, the absorption peaks near 2954 cm^{-1} are the stretching vibration absorption peaks of $-CH_2$ and $-CH_3$, and the absorption peaks near 1535 cm^{-1} are the deformation vibration peaks of the benzene ring backbone and the backbone vibration peaks of the imidazole ring. The absorption peaks near 1680 cm^{-1} are the C═O stretching vibration, and the absorption peak near 1439 cm^{-1} is the C−N stretching vibration peak in the amide group and the out-of-plane bending vibration peaks of $-CH_2$ and $-CH_3$. All of the characteristic groups of functional monomers have the corresponding absorption peaks in MICs, indicating that the corresponding functional monomers were successfully introduced into MICs. In addition, the infrared spectra of MICs and NICs are basically the same, suggesting that the BSA in the prepared MICs had been completely eluted.

The chemical structures of the synthesized MICs were further confirmed using X-ray photoelectron spectroscopy (XPS), and the results are shown in Figure 3. From the XPS broad sweep spectrum of MICs in Figure 3b, it can be seen that the O 1s peak at a binding energy of 529.7 eV, the N 1s peak at 400.8 eV, the C 1s peak at 284.7 eV, the S 2p peak at 164.2 eV, and the P 2p peak at 130.4 eV appear in the spectrum, which indicates that there are five elements (O, C, N, S, and P) in the MICs. The C 1s and N 1s energy spectra of MICs are processed by XPS peak fitting, and the results are shown in Figure 3c,d. In Figure 3c, the C 1s peak at 284.5 eV is attributed to the C−H bond, the C 1s peak at 285.7 eV is attributed to the C−N bond, the C 1s peak at 287.0 eV is attributed to the C═C bond, the C 1s peak at 287.6 eV is attributed to the C═O bond, the C 1s peak at 288.1 eV is attributed to the C═N bond, and the C 1s peak at 288.8 eV is attributed to the C−S═O bonds, which correspond to the six forms of C in MICs, respectively. Figure 3d shows two peaks of N 1s at 398.6 and 401.7 eV attributed to the two N atoms of the imidazole moiety and the characteristic peak at 400.5 eV attributed to the N atoms contained in the amide moiety. The structures of the prepared MICs can be determined from the FT-IR and XPS results.

3.3. Microscopic Morphology of MICs. A scanning electron microscope was used to observe the microscopic morphology of the prepared MICs and NICs, respectively, and the results are shown in Figure 4. Figure 4a–c shows that the MICs exhibit a three-dimensional network structure with a pore size distribution between 10 and 20 μm larger than that of the NICs (5–10 μm) in Figure 4d–f. The porous structure can effectively reduce the mass transfer resistance during the protein recognition process and improve the recognition adsorption and elution of proteins.[44,45] Through a combination of SEM and energy-dispersive spectroscopy (EDS), the MICs can also be rapidly analyzed in terms of elemental

https://doi.org/10.1021/acsomega.4c11143
ACS Omega 2025, 10, 11312−11324

species and content. The EDS of MICs and NICs and the corresponding elemental contents are shown in Figure 4g,h and Table 2. As shown in Table 2, MICs and NICs contain

Table 2. Surface Atomic Compositions of MICs and NICs

sample	atomic concentration (atomic %)					
	C	N	O	P	S	Cl
MICs	47.53	18.64	27.31	3.19	1.58	1.74
NICs	48.51	15.26	24.49	2.73	3.91	5.10

47.53% C, 18.64% N, 27.31% O, and a small amount of P and S elements, which is basically consistent with the contents of several functional monomers and cross-linking agents. The above conclusions are basically consistent with those obtained by XPS, which shows that the functional monomers and cross-linkers have participated in the synthesis of MICs materials.

3.4. Thermal Stability and Temperature Sensitivity Studies of MICs. Thermogravimetric analysis (TGA) and differential scanning calorimetry (DSC) were used to characterize the thermal stability of the MICs and NICs, and the results are shown in Figure 5. The thermal weight loss curves of MICs and NICs in Figure 5a are basically the same, and when the temperature is increased from 25 to 100 °C, the MICs and NICs lost 8.9% mass, which is most likely due to the mass loss of water adsorbed on the surface of the materials. When the temperature is in the range of 100−240 °C, the MICs and NICs have almost no mass loss. However, significant mass loss of MICs and NICs occurs when the temperature is higher than 240 °C, which is caused by decomposition of the polymer chains of MICs and NICs. From the results of TGA, it can be seen that the prepared MIC materials have good thermal stability when the temperature is no higher than 240 °C.

In this study, temperature-sensitive MICs were prepared by freeze polymerization in the presence of an aqueous-phase cross-linking agent[*N*,*N*-methylenebis(acrylamide)], ionic liquid ([$P_{4,4,4,4}$][SS]) as the temperature-sensitive monomer, and [VAFMIM]Cl and AM as the cofunctional monomers. The LCST-type ionic liquids [$P_{4,4,4,4}$][SS] is characterized by exhibiting hydrophilicity below LCST and hydrophobicity above LCST, which can be clearly seen from Figure 5b. It can be clearly seen from Figure 5b that when the temperature is lower than that of LCST (36 °C), [$P_{4,4,4,4}$][SS] has a good affinity with water, making the solution a transparent homogeneous solution. When the temperature is higher than that of LCST (36 °C), the hydrophobicity of [$P_{4,4,4,4}$][SS] is enhanced and precipitated from the aqueous solution. By introducing this monomer, the prepared MICs also acquire temperature sensitivity. The MICs are in a swollen state when the temperature is below LCST and in a contracted state when the temperature is above LCST. The contraction and swelling of the volume of MIC materials are controlled by adjusting temperature to achieve specific recognition or efficient elution of target proteins.[46−48] Differential scanning calorimetry (DSC) was used to study the temperature sensitivity of MICs and NICs by determining their enthalpies of phase transitions, and the results are shown in Figure 5c. As shown in Figure 5c, there is a clear heat absorption peak at 58 °C for MICs and NICs, which is the lowest critical phase transition temperature (LCST) for both. Compared with the phase transition temperature of [$P_{4,4,4,4}$][SS] monomer solution at 36 °C, the LCST of both MICs and NICs increases, which may be related to the polymerization of [$P_{4,4,4,4}$][SS]. In addition, [VAFMIM]Cl and AM monomers containing hydrophilic groups are involved in the polymerization of MICs, and these monomers have a strong influence on the hydrophilic and hydrophobic properties of MICs. The temperature sensitivity of the materials will provide a favorable aid to the mass transfer, movement, and accurate localization of large proteins during blotting, elution, and recognition.

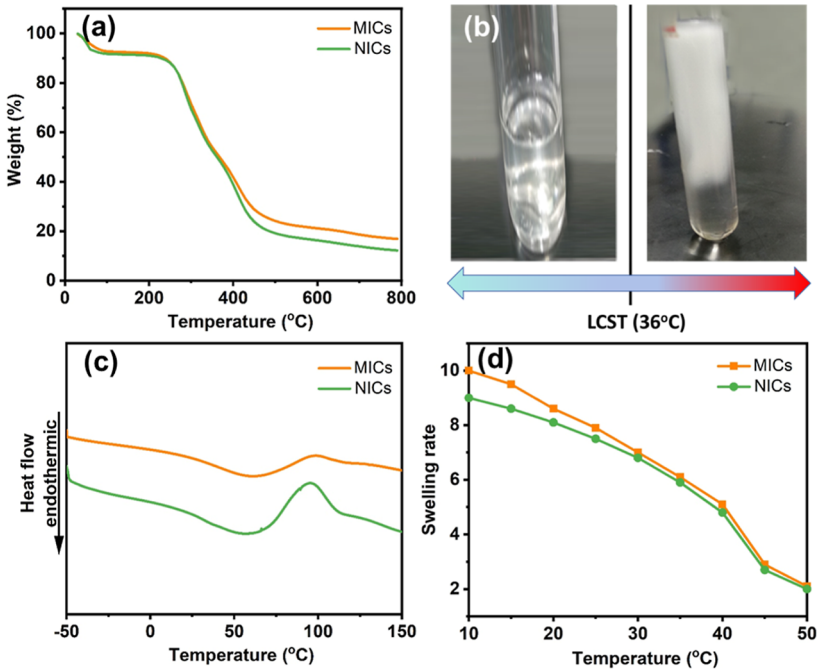

Figure 5. (a) TGA curves of MICs and NICs; (b) picture illustrations of the LCST-type phase transition of [$P_{4,4,4,4}$][SS] solution taken at temperatures below and above LCST; (c) DSC curves for MICs and NICs; (d) effect of temperature on the swelling ratio of MICs and NICs.

https://doi.org/10.1021/acsomega.4c11143
ACS Omega 2025, 10, 11312−11324

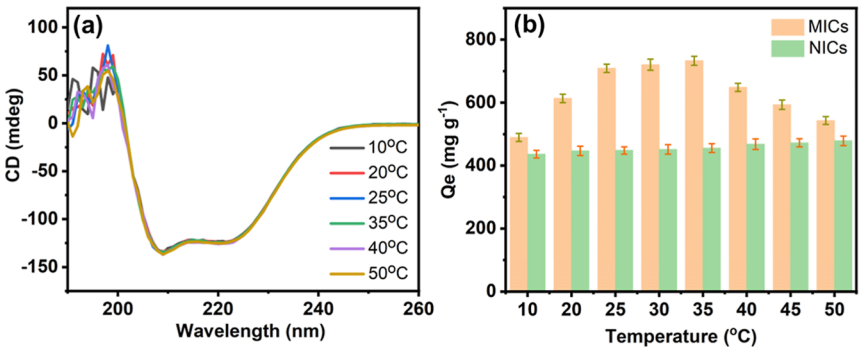

Figure 6. (a) CD spectrum of BSA at different temperatures; (b) effect of temperature on adsorption ability of MICs and NICs.

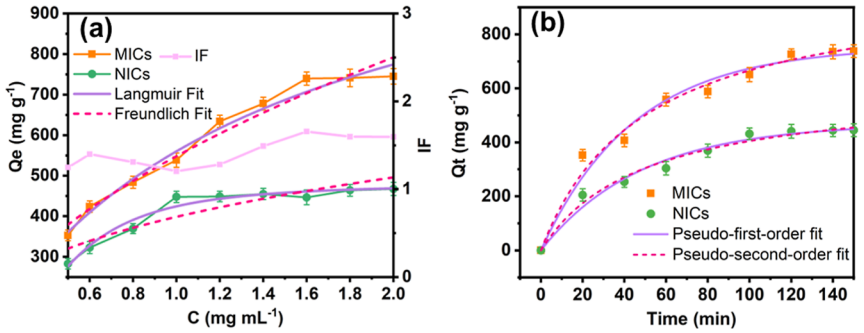

Figure 7. (a) Adsorption isotherms curves of MICs and NICs for BSA at 25 °C; (b) adsorption kinetic curves of MICs and NICs for BSA at 25 °C.

To further investigate the sensitivity of the MICs to temperature, the effect of temperature on the swelling rate of the MICs and NICs in PBS (0.01 mol L^{-1}, pH = 7.4) was investigated, and the results are shown in Figure 5d. As can be seen in Figure 5d, when the temperature is 10 °C, a more substantial swelling in the volume of MICs occurs due to the fact that the anionic groups of the temperature-sensitive ionic liquid ($[P_{4,4,4,4}][SS]$) are able to generate stable interactions with water molecules by hydrogen bond at low temperatures, which allows the water molecules to be inserted between the chain segments. When the temperature gradually increases, the solubility of the MICs decreases continuously. Especially when the temperature reaches 40 °C, the volume of MICs undergoes a significant shrinkage, which is consistent with the results of the phase transition of DSC. For this heat-shrinkable temperature-sensitive MICs, when the ambient temperature is lower than its LCST, the MICs in the swollen state contribute to the mass transfer and elution of protein molecules. However, the imprinted sites on the polymer chain segments are far from each other, which is not conducive to the accurate identification of proteins. When the ambient temperature is higher than its LCST, the cryogel undergoes obvious contraction, and structure collapses, which is also unfavorable to the process of protein binding and recognition. When the ambient temperature is near the LCST, the structure of the imprinting pores can be maintained, which is helpful for the efficient and accurate recognition of target protein molecules.

3.5. Effect of Temperature on the Adsorption Properties of MICs. The MIC materials prepared with LCST-type ionic liquids ($[P_{4,4,4,4}][SS]$) as functional monomers can sense the external temperature to undergo reversible volume changes and adjust the adsorption performance of the imprinted materials for the target proteins. As shown in Figure 6a, the CD spectra of BSA in the temperature range 10−50 °C are not significantly different, showing the stability of the BSA structure in the experimental temperature range. Figure 6b shows the adsorption properties of MICs and NICs on BSA at different temperatures. It can be seen that the adsorption capacity of MICs on BSA first increases and then decreases with the increase of the temperature and reaches the maximum adsorption at 37 °C. Combined with the results of DSC and swelling rate, the shrinkage that occurred in the volume of MICs in the range of 10 to 50 °C causes the imprinted cavities to undergo volume changes as well. At 35 °C, the shape of the cavities and the distribution of charged groups should be highly matched to those of the protein, resulting in the highest affinity. When the temperature is increased to 50 °C, disruption of the polymer network leads to disruption of the spatial integrity of the recognition sites, making it difficult for the target proteins to bind to the imprinting sites and decreasing the adsorption capacity. Besides, due to the existence of LCST-type ionic liquid ($[P_{4,4,4,4}][SS]$) functional monomers, the hydrophilicity/hydrophobicity of the prepared polymer cryogel material will change with the change of temperature, which will also affect the adsorption of proteins. The difference of hydrophilic/hydrophobic properties will have an impact on the adsorption kinetics and adsorption model of the cryogel material, which will be discussed in detail in the following content. The nonspecific adsorption of NICs to BSA increases slightly with increasing temperature, which may be related to the increased hydrophobicity of the cryogel enhancing the interaction with proteins.[47,49] The adsorption capacity of MICs at 25 °C is similar to that at 35 °C, and the low temperature is more conducive to mass transfer and elution of proteins. Therefore, the adsorption experiments of the imprinted cryogel materials for BSA in this study were carried out in the adsorption solution at 25 °C.

https://doi.org/10.1021/acsomega.4c11143
ACS Omega 2025, 10, 11312−11324

Table 3. Isotherm Models and Constants of MICs and NICs for Target Protein BSA

isotherm model	Langmuir			Freundlich		
materials	Q_{max} (mg g^{-1})	K_L (L·mg^{-1})	R^2	K_F (mg g^{-1})	n	R^2
MICs	1254.82	1.9510	0.9843	547.99	1.8816	0.9711
NICs	479.43.33	0.7781	0.9606	398.32	3.1726	0.8191

Table 4. Fitting Parameters of the Pseudo-First-Order and Pseudo-Second-Order Dynamics Models

		pseudo-first-order			pseudo-second-order		
materials	Q_e (mg g^{-1})	$Q_{e,c}$ (mg g^{-1})	k_1 (min^{-1})	R^2	$Q_{e,c}$ (mg g^{-1})	k_2 (g mg^{-1} min^{-1})	R^2
MICs	736.47	754.54	0.0223	0.9766	995.13	0.00002	0.9968
NICs	424.85	470.06	0.0207	0.9790	604.56	0.00003	0.9833

3.6. Adsorption Isotherm and Imprinting Efficiency.

The MICs that can recognize the target protein (BSA) were prepared by cryopolymerization using BSA as a template, and their isothermal adsorption behaviors were investigated at 25 °C, as shown in Figure 7a. From Figure 7a, it can be seen that the adsorption of BSA by both MICs and NICs increases with the increase of BSA concentration and finally tends to the saturation adsorption (Q_e). The saturation adsorption of BSA by MICs and NICs is 741.5 and 449.8 mg g^{-1}, respectively, with the maximum imprinting factor (IF) of 1.65. The experimental results show that the MICs have a greater adsorption capacity for BSA in the same concentration. Compared with NICs with the same components, the additional adsorption capacity of MICs comes from multiple interactions, such as hydrogen bonding, $\pi-\pi$ conjugation, hydrophobicity, and electrostatic interactions between multiple functional monomers and many amino acid residues of BSA, which forms a large number of imprinting sites in MICs that matches with BSA and enlarges the adsorption capacity.[35,50]

Adsorption behavior can be studied using Langmuir and Freundlich isothermal models, as shown in eqs 5 and 6.

$$\frac{C_e}{Q_e} = \frac{C_e}{Q_{max}} + \frac{1}{K_L Q_{max}} \quad (5)$$

$$Q_e = K_F C_e^{1/n} \quad (6)$$

where C_e (mg mL^{-1}) is the concentration of BSA at adsorption equilibrium, Q_e (mg g^{-1}) is the experimental saturated adsorption capacity of BSA, Q_{max} (mg g^{-1}) is the theoretical maximum adsorption capacity of BSA, and K_L (L mg^{-1}) and K_F (mg g^{-1}) are adsorption equilibrium constants in the Langmuir isotherm equation and the Freundlich isotherm equation, respectively. The adsorption equilibrium constant and n are constants describing the strength of adsorption. The Langmuir model and the Freundlich model describe adsorption on a uniform surface with a uniform active site and a nonuniform surface with an exponential distribution of active sites, respectively. The fitted parameters of the Langmuir and Freundlich isothermal adsorption models are shown in Table 3, respectively. By comparing the R^2 values of the correlation coefficients, the correlation coefficient fitted by the Langmuir adsorption isothermal equation (0.9843) is larger than that fitted by the Freundlich adsorption isothermal equation (0.9711), which indicates that the adsorption behavior of the MICs on the template protein BSA is more in line with the Langmuir model, demonstrating that the adsorption of MICs on BSA is more in line with the monomolecular layer adsorption.[46] Due to the pore size of MICs prepared under freezing conditions is larger, the target protein BSA has less resistance during the transmission process, and BSA tends to be recognized by the uniformly distributed imprinted sites in MICs, so the adsorption of MICs on BSA is closer to the adsorption behavior described by the Langmuir adsorption model.[46,51] In addition, a comparison of Langmuir adsorption equilibrium constants K_L revealed that the K_L value of MICs was higher than that of NICs, which indicates that the adsorption ability of MICs for the target protein BSA is stronger than that of NICs, and also proves that more precise BSA imprinting sites were formed during the preparation of MIC materials.[52]

3.7. Adsorption Kinetics Study of MICs and NICs.

Adsorption kinetics was used to study the rate of adsorption of molecularly imprinted materials for target molecules and the time taken to reach adsorption equilibrium. Figure 7b shows the adsorption kinetics of MICs and NICs to BSA in a BSA solution at a concentration of 1.6 mg mL^{-1} at 25 °C.

As can be seen from Figure 7b, the adsorption of MICs on the template protein BSA shows a trend of rapid increase in the first 20 min, then the adsorption of MICs on BSA slows down from 20 to 100 min, and the adsorption of MICs on BSA tends to be in equilibrium when the adsorption time reaches 125 min. Compared with the adsorption of MICs on the template protein BSA, the adsorption capacity of NICs on BSA is lower and shows a slow growth trend with time and basically reached adsorption saturation at 100 min. This is related to the fact that MICs have a large specific surface area, a large pore size, and more imprinted sites, which makes the material have a high mass transfer capacity to the target protein.

The adsorption behavior was studied by means of pseudo-first-order and pseudo-second-order kinetic models shown in eqs 7 and 8.

$$\ln(Q_e - Q_t) = \ln Q_e - k_1 t \quad (7)$$

$$\frac{t}{Q_t} = \frac{1}{k_2 Q_e^2} + \frac{t}{Q_e} \quad (8)$$

where Q_t and Q_e are the adsorption capacity (mg g^{-1}) at any time and at adsorption equilibrium, respectively. k_1 and k_2 are the rate constants for the pseudo-first-order kinetic equation (min^{-1}) and the pseudo-second-order kinetic equation (g mg^{-1} min^{-1}), respectively. The fitted parameters of the pseudo-first-order kinetic equation (min^{-1}) and the pseudo-second-order kinetic equation (g mg^{-1} min^{-1}) for BSA adsorption by MICs and NICs are shown in Table 4. The correlation coefficients R^2 of the pseudo-first-order kinetic equation and the pseudo-second-order kinetic equation for the adsorption of MICs to BSA in Table 4 are 0.9766 and 0.9968,

https://doi.org/10.1021/acsomega.4c11143
ACS Omega 2025, 10, 11312−11324

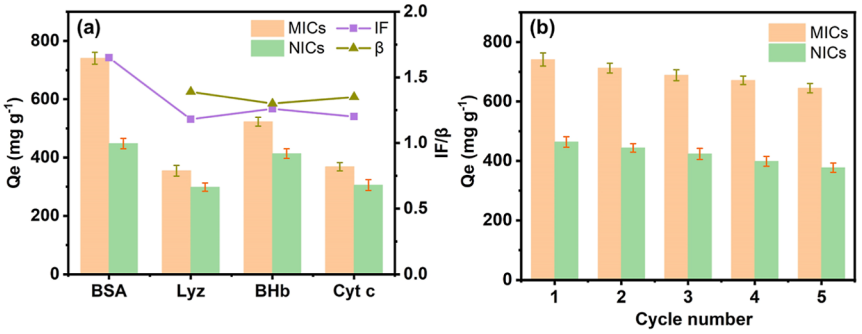

Figure 8. (a) Recognition performance of MICs and NICs for different proteins; (b) recycling performance of MICs and NICs.

respectively, indicating that the pseudo-second-order kinetics can more accurately describe the adsorption control mechanism of MICs. Similar to MICs, the correlation coefficient R^2 of the pseudo-second-order kinetic equation for NICs is slightly higher than that of the pseudo-first-order kinetic equation, indicating that MICs and NICs have the same adsorption control mechanism.

3.8. Specific Recognition Properties of MICs for BSA. The specific recognition performance of MICs for the template protein BSA was investigated by comparing the adsorption amount and selectivity factor (β) of MICs for the three contrasting proteins (Lyz, BHb, and Cyt *c*). The results are listed in Figure 8a.

The adsorption capacity of MICs for Lyz, BHb and Cyt *c* in Figure 8a is much lower than that of BSA, indicating that imprinted sites with memory function for BSA formed in MICs are more conducive to the specific recognition and adsorption of BSA. Among them, the higher adsorption of BHb by MICs could be attributed to the fact that BHb has a similar molecular weight (64.7 kDa) and isoelectric point (6.9) to the template protein BSA and has a net positive charge in the adsorbent solution at pH 7.4, which is in favor of nonspecific adsorption caused by electrostatic and hydrogen bonding interactions with *p*-styrenesulfonate-based anions in the MICs. The selection factor (β) in Figure 8a shows that the specific recognition of BSA by MICs is 1.39, 1.3, and 1.35 times higher than that of Lyz, BHb, and Cyt *c*, respectively, indicating that the prepared MICs have better specific recognition performance for the target protein BSA. This is mainly due to the existence of a large number of imprinted sites in MICs in the preparation of imprinted materials under freezing conditions that match with BSA, which improves the specific recognition of BSA through multiple interactions such as hydrogen bonding, $\pi-\pi$ conjugation, hydrophobicity, and electrostatic interaction. Meanwhile, the macroporous structure of cryogel promotes the mass transfer of protein molecules and facilitates the proximity and interaction of target proteins to the imprinted sites.

3.9. Recycling Performance of MICs. The cyclic regeneration performance of MICs was investigated by cyclic adsorption−desorption experiments, and the results are shown in Figure 8b. As can be seen in Figure 8b, the adsorption of BSA by the MICs decreased by 13.02% after five cycles. The lost adsorption amount may be due to the fact that the macropore structure of MICs is easily destroyed during cycling, reducing the effective adsorption sites and making the imprinted pore unable to effectively recognize the template protein. The results show that the imprinted pores of the MICs have sufficient stability to maintain a high adsorption capacity after many cycles of use. From the above analysis, it can be concluded that MICs have excellent regeneration and reusability and have the potential for practical application in protein separation.

3.10. Adsorption Performance in a Real Sample. In order to study the selective adsorption performance of MICs in real samples, adsorption experiments of MICs and NICs in real bovine serum samples were carried out. The adsorption of MICs and NICs to proteins in real bovine serum was analyzed by sodium dodecyl sulfate polyacrylamide gel electrophoresis (SDS-PAGE), and the results are shown in Figure 9. As shown in Figure 9, lane 2 is the result of the bovine serum solution containing BSA (66.4 kDa). Lane 3 and lane 4, respectively, display that the intensity of BSA eluted from MICs and NICs after adsorption in the bovine serum solution. Compared to the intensity of the band for BSA eluted from MICs in lane 4, the intensity of the band for BSA eluted from MICs in lane 3 is much higher, which is almost as high as that in lane 2. These results explain that the adsorption ability of MICs for BSA in real bovine serum samples is significantly higher than that of corresponding NICs, showing an excellent application ability of adsorption and separation of target protein (BSA) in real biological samples.

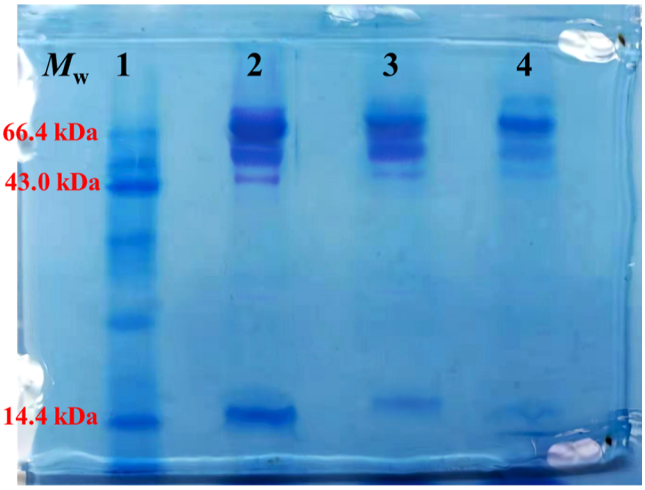

Figure 9. SDS-PAGE results of competition experiment (Lane 1, protein molecular weight marker; lane 2, PBS diluent of bovine serum and BSA; lane 3, proteins eluted from MICs; lane 4, proteins eluted from NICs).

https://doi.org/10.1021/acsomega.4c11143
ACS Omega 2025, 10, 11312−11324

4. CONCLUSIONS

In this study, temperature-sensitive MICs were prepared by freeze polymerization in the presence of an aqueous-phase cross-linking agent using BSA as a template molecule, LCST-type ionic liquids ([$P_{4,4,4,4}$][SS]) as temperature-sensitive monomers used in response to changes in external temperature, and imidazolium-type ionic liquids ([VAFMIM]Cl) and AM as cofunctional monomers. The three-dimensional macroporous structure of MICs can effectively reduce the mass transfer resistance of proteins in the recognition process and improve the recognition, adsorption, and elution of proteins. The adsorption performance of MICs is temperature-sensitive, and the adsorption capacity of the MICs on BSA changes with the increase of the temperature and reaches the maximal adsorption capacity at 37 °C. The saturated adsorption capacity of the MICs is about 741.5 mg g^{-1}, and the imprint factor is 1.65, which is consistent with the isothermal adsorption behavior being more in accordance with the Langmuir model. The adsorption amounts of MICs on Lyz, BHb and Cyt *c* are much lower than that of BSA, which showed excellent specific recognition ability. The adsorption capacity of MICs on BSA is still as high as 86.98% after 5 adsorption−desorption cycles, which is an excellent recycling performance.

■ ASSOCIATED CONTENT

Supporting Information

The Supporting Information is available free of charge at https://pubs.acs.org/doi/10.1021/acsomega.4c11143.

The structural characterization of *p*-styrenesulfonic acid tetrabutylphosphine salt ionic liquids ([$P_{4,4,4,4}$][SS]); structural characterization of 1-vinyl-3-carbamoylmethylimidazole chloride salt ionic liquids ([VAFMIM]Cl); determination of BSA solution concentration; study on kinetic adsorption of MICs; effect of acrylamide (AM) on the adsorption of MICs and NICs to BSA; research on the specific recognition performance of MICs; study on competitive adsorption of MICs; and recycling performance of MICs (PDF)

■ AUTHOR INFORMATION

Corresponding Authors

Dandan Cheng − *School of Life Science, Wuchang University of Technology, Wuhan 430223, P. R. China;* orcid.org/0009-0000-5882-4895; Email: chengdandan135@163.com

Zhao Zhao − *School of Life Science, Wuchang University of Technology, Wuhan 430223, P. R. China;* Email: 18297195862@139.com

Authors

Yahong Chen − *School of Life Science, Wuchang University of Technology, Wuhan 430223, P. R. China*

Yalan Feng − *School of Life Science, Wuchang University of Technology, Wuhan 430223, P. R. China*

Yijun Zeng − *School of Life Science, Wuchang University of Technology, Wuhan 430223, P. R. China*

Complete contact information is available at: https://pubs.acs.org/10.1021/acsomega.4c11143

Author Contributions

Dandan Cheng: Conceptualization, methodology, writing—original draft, and writing−review and editing. Yahong Chen: Methodology and writing—original draft. Yalan Feng: Visualization and formal analysis. Yijun Zeng: Data curation and investigation. Zhao Zhao: Project administration and funding acquisition.

Notes

The authors declare no competing financial interest.

■ ACKNOWLEDGMENTS

The authors express gratitude for the financial support provided by 2021 Hubei Provincial universities outstanding young and middle-aged science and technology Innovation team project (T2021041).

■ REFERENCES

(1) Arabi, M.; Ostovan, A.; Li, J.; Wang, X.; Zhang, Z.; Choo, J.; Chen, L. Molecular imprinting: green perspectives and strategies. *Adv. Mater.* **2021**, *33*, 2100543.

(2) Zhang, W.; Zhang, Y.; Wang, R.; Zhang, P.; Zhang, Y.; Randell, E.; Zhang, M.; Jia, Q. A review: Development and application of surface molecularly imprinted polymers toward amino acids, peptides, and proteins. *Anal. Chim. Acta* **2022**, *1234*, 340319.

(3) Jahanban-Esfahlan, A.; Roufegarinejad, L.; Jahanban-Esfahlan, R.; Tabibiazar, M.; Amarowicz, R. Latest developments in the detection and separation of bovine serum albumin using molecularly imprinted polymers. *Talanta* **2020**, *207*, 120317.

(4) He, Y.; Lin, Z. Recent advances in protein-imprinted polymers: synthesis, applications and challenges. *J. Mater. Chem. B* **2022**, *10*, 6571−6589.

(5) Akgönüllü, S.; Kılıç, S.; Esen, C.; Denizli, A. Molecularly imprinted polymer-based sensors for protein detection. *Polymers* **2023**, *15*, 629.

(6) Xing, R.; Guo, Z.; Lu, H.; Zhang, Q.; Liu, Z. Molecular imprinting and cladding produces antibody mimics with significantly improved affinity and specificity. *Sci. Bull.* **2022**, *67*, 278−287.

(7) Reville, E. K.; Sylvester, E. H.; Benware, S. J.; Negi, S. S.; Berda, E. B. Customizable molecular recognition: Advancements in design, synthesis, and application of molecularly imprinted polymers. *Polym. Chem.* **2022**, *13*, 3387−3411.

(8) Murdaya, N.; Triadenda, A. L.; Rahayu, D.; Hasanah, A. N. A review: using multiple templates for molecular imprinted polymer: is it good? *Polymers* **2022**, *14*, 4441.

(9) Memic, A.; Colombani, T.; Eggermont, L. J.; Rezaeeyazdi, M.; Steingold, J.; Rogers, Z. J.; Navare, K. J.; Mohammed, H. S.; Bencherif, S. A. Latest advances in cryogel technology for biomedical applications. *Adv. Ther.* **2019**, *2*, 1800114.

(10) Fan, J.-P.; Dong, W.-Y.; Zhang, X.-H.; Yu, J.-X.; Huang, C.-B.; Deng, L.-J.; Chen, H.-P.; Peng, H.-L. Preparation and characterization of protein molecularly imprinted poly (ionic liquid)/calcium alginate composite cryogel membrane with high mechanical strength for the separation of bovine serum albumin. *Molecules* **2022**, *27*, 7304.

(11) Idumah, C. I. Recently emerging advancements in polymeric cryogel nanostructures and biomedical applications. *Int. J. Polym. Mater. Polym. Biomater.* **2023**, *72*, 1307−1327.

(12) Wardani, N. I.; Kangkamano, T.; Wannapob, R.; Kanatharana, P.; Thavarungkul, P.; Limbut, W. Electrochemical sensor based on molecularly imprinted polymer cryogel and multiwalled carbon nanotubes for direct insulin detection. *Talanta* **2023**, *254*, 124137.

(13) Öztürk, G.; Saylan, Y.; Denizli, A. Designing composite cryogel carriers for tyrosine adsorption. *Sep. Purif. Technol.* **2021**, *254*, 117622.

(14) Bakhshpour, M.; Göktürk, I.; Bereli, N.; Denizli, A. Molecularly imprinted cryogel cartridges for the selective recognition of tyrosine. *Biotechnol. Prog.* **2020**, *36*, No. e3006.

(15) Andaç, M.; Galaev, I. Y.; Denizli, A. Affinity based and molecularly imprinted cryogels: Applications in biomacromolecule purification. *J. Chromatogr. B* **2016**, *1021*, 69−80.
(16) Kartal, F.; Denizli, A. Molecularly imprinted cryogel beads for cholesterol removal from milk samples. *Colloids Surf., B* **2020**, *190*, 110860.
(17) Zenger, O.; Peşint, G. B. Preparation of molecularly imprinted bilayer cryogel columns for selective protein depletion. *Process Biochem.* **2022**, *117*, 90−100.
(18) Karaduman, A. B.; Çetin, K. Molecularly imprinted cryogels for the selective adsorption of salicylic acid. *Appl. Biochem. Biotechnol.* **2023**, *195*, 1877−1887.
(19) Canpolat, G.; Dolak, I. ·.; Onat, R.; Keçili, R.; Baysal, Z.; Ziyadanoğulları, B.; Ersöz, A.; Say, R. Development of molecular imprinting-based smart cryogels for selective recognition and separation of serum cytochrome-c as a biochemical indicator. *Process Biochem.* **2021**, *106*, 112−119.
(20) Shiekh, P. A.; Andrabi, S. M.; Singh, A.; Majumder, S.; Kumar, A. Designing cryogels through cryostructuring of polymeric matrices for biomedical applications. *Eur. Polym. J.* **2021**, *144*, 110234.
(21) Asena Özbek, M.; Özgür, E.; Bereli, N.; Denizli, A. Molecular imprinted based microcryogels for thrombin purification. *J. Chromatogr. B* **2023**, *1228*, 123848.
(22) Aslıyüce, S.; Idil, N.; Mattiasson, B. Upgrading of bio-separation and bioanalysis using synthetic polymers: Molecularly imprinted polymers (MIPs), cryogels, stimuli-responsive polymers. *Eng. Life Sci.* **2022**, *22*, 204−216.
(23) Ulusoy, M.; Aslıyüce, S.; Keskin, N.; Denizli, A. Beauvericin purification from fungal strain using molecularly imprinted cryogels. *Process Biochem.* **2022**, *113*, 185−193.
(24) Dolak, I. ·.; Canpolat, G.; Onat, R.; Keçili, R.; Baysal, Z.; Ziyadanoğulları, B.; Ersöz, A.; Say, R. A novel lanthanide-chelate based molecularly imprinted cryogel for purification of hemoglobin from blood serum: An alternative method for thalassemia diagnosis. *Process Biochem.* **2020**, *91*, 189−196.
(25) Yang, Z.; Zhang, Y.; Ren, J.; Zhang, Q.; Zhang, B. Cobalt-iron double ion-bovine serum albumin chelation-assisted thermo-sensitive surface-imprinted nanocage with high specificity. *ACS Appl. Mater. Interfaces* **2021**, *13*, 34829−34842.
(26) Zhang, Y.; Wang, Q.; Zhao, X.; Ma, Y.; Zhang, H.; Pan, G. Molecularly imprinted nanomaterials with stimuli responsiveness for applications in biomedicine. *Molecules* **2023**, *28*, 918.
(27) Morsi, S. M.; Abd El-Aziz, M. E.; Mohamed, H. A. Smart polymers as molecular imprinted polymers for recognition of target molecules. *Int. J. Polym. Mater. Polym. Biomater.* **2023**, *72*, 612−635.
(28) Jain, A.; Bajpai, J.; Bajpai, A.; Mishra, A. Thermoresponsive cryogels of poly (2-hydroxyethyl methacrylate-co-N-isopropyl acrylamide)(P (HEMA-co-NIPAM)): fabrication, characterization and water sorption study. *Polym. Bull.* **2020**, *77*, 4417−4443.
(29) Picos-Corrales, L. A.; Morales-Burgos, A. M.; Ruelas-Leyva, J. P.; Crini, G.; García-Armenta, E.; Jimenez-Lam, S. A.; Ayón-Reyna, L. E.; Rocha-Alonzo, F.; Calderón-Zamora, L.; Osuna-Martínez, U.; et al. Chitosan as an outstanding polysaccharide improving health-commodities of humans and environmental protection. *Polymers* **2023**, *15*, 526.
(30) Setia, A.; Sahu, R. K.; Ray, S.; Widyowati, R.; Ekasari, W.; Saraf, S. Advances in hybrid vesicular-based drug delivery systems: improved biocompatibility, targeting, therapeutic efficacy and pharmacokinetics of anticancer drugs. *Curr. Drug Metab.* **2022**, *23*, 757−780.
(31) Maity, S.; Gaur, D.; Mishra, B.; Dubey, N. C.; Tripathi, B. P. Bactericidal and biocatalytic temperature responsive microgel based self-cleaning membranes for water purification. *J. Colloid Interface Sci.* **2023**, *642*, 129−144.
(32) Wilms, D.; Schröer, F.; Paul, T. J.; Schmidt, S. Switchable adhesion of E. coli to thermosensitive carbohydrate-presenting microgel layers: A single-cell force spectroscopy study. *Langmuir* **2020**, *36*, 12555−12562.
(33) Chen, H.; Yu, C.; Wu, H.; Li, G.; Li, C.; Hong, W.; Yang, X.; Wang, H.; You, X. Recent advances in histidine kinase-targeted antimicrobial agents. *Front. Chem.* **2022**, *10*, 866392.
(34) Ayon, N. J. High-throughput screening of natural product and synthetic molecule libraries for antibacterial drug discovery. *Metabolites* **2023**, *13*, 625.
(35) Wang, Y.; Ma, Y.; Zhou, J.; Su, K.; Zhang, B.; Zhang, Q. Thermo-sensitive surface molecularly imprinted magnetic micro-spheres based on bio-macromolecules and their specific recognition of bovine serum albumin. *J. Sep. Sci.* **2020**, *43*, 996−1002.
(36) Boukadida, M.; Anene, A.; Jaoued-Grayaa, N.; Chevalier, Y.; Hbaieb, S. Choice of the functional monomer of molecularly imprinted polymers: Does it rely on strong acid-base or hydrogen bonding interactions? *Colloid and Interface Science Communications* **2022**, *50*, 100669.
(37) Thach, U. D.; Nguyen Thi, H. H.; Pham, T. D.; Mai, H. D.; Nhu-Trang, T.-T. Synergetic effect of dual functional monomers in molecularly imprinted polymer preparation for selective solid phase extraction of ciprofloxacin. *Polymers* **2021**, *13*, 2788.
(38) El-Sharif, H. F.; Turner, N. W.; Reddy, S. M.; Sullivan, M. V. Application of thymine-based nucleobase-modified acrylamide as a functional co-monomer in electropolymerised thin-film molecularly imprinted polymer (MIP) for selective protein (haemoglobin) binding. *Talanta* **2022**, *240*, 123158.
(39) Resina, L.; Alemán, C.; Ferreira, F. C.; Esteves, T. Protein-imprinted polymers: How far have "plastic antibodies" come? *Biotechnol. Adv.* **2023**, *68*, 108220.
(40) Xie, L.; Xiao, N.; Li, L.; Xie, X.; Li, Y. Theoretical insight into the interaction between chloramphenicol and functional monomer (methacrylic acid) in molecularly imprinted polymers. *Int. J. Mol. Sci.* **2020**, *21*, 4139.
(41) Hasanah, A. N.; Safitri, N.; Zulfa, A.; Neli, N.; Rahayu, D. Factors affecting preparation of molecularly imprinted polymer and methods on finding template-monomer interaction as the key of selective properties of the materials. *Molecules* **2021**, *26*, 5612.
(42) Pasquardini, L.; Bossi, A. M. Molecularly imprinted polymers by epitope imprinting: a journey from molecular interactions to the available bioinformatics resources to scout for epitope templates. *Anal. Bioanal. Chem.* **2021**, *413*, 6101−6115.
(43) Tse Sum Bui, B.; Mier, A.; Haupt, K. Molecularly imprinted polymers as synthetic antibodies for protein recognition: the next generation. *Small* **2023**, *19*, 2206453.
(44) Liang, C.; Zhang, Z.; Zhang, H.; Ye, L.; He, J.; Ou, J.; Wu, Q. Ordered macroporous molecularly imprinted polymers prepared by a surface imprinting method and their applications to the direct extraction of flavonoids from Gingko leaves. *Food Chem.* **2020**, *309*, 125680.
(45) Bhogal, S.; Kaur, K.; Mohiuddin, I.; Kumar, S.; Lee, J.; Brown, R. J.; Kim, K.-H.; Malik, A. K. Hollow porous molecularly imprinted polymers as emerging adsorbents. *Environ. Pollut.* **2021**, *288*, 117775.
(46) Cao, J.; Wu, X.; Wang, L.; Shao, G.; Qin, B.; Wang, Z.; Wang, T.; Fu, Y. A cellulose-based temperature sensitivity molecular imprinted hydrogel for specific recognition and enrichment of paclitaxel. *Int. J. Biol. Macromol.* **2021**, *181*, 1231−1242.
(47) Toyoshima, Y.; Kawamura, A.; Takashima, Y.; Miyata, T. Design of molecularly imprinted hydrogels with thermoresponsive drug binding sites. *J. Mater. Chem. B* **2022**, *10*, 6644−6654.
(48) Liu, Y.; Hu, X.; Liu, Z.; Meng, M.; Pan, J.; Jiang, Y.; Ni, L.; Wu, W. A novel dual temperature responsive mesoporous imprinted polymer for Cd (II) adsorption and temperature switchable controlled separation and regeneration. *Chem. Eng. J.* **2017**, *328*, 11−24.
(49) Turan, E.; Özçetin, G.; Caykara, T. Dependence of Protein Recognition of Temperature-Sensitive Imprinted Hydrogels on Preparation Temperature. *Macromol. Biosci.* **2009**, *9*, 421−428.
(50) Ran, D.; Wang, Y.; Jia, X.; Nie, C. Bovine serum albumin recognition via thermosensitive molecular imprinted macroporous hydrogels prepared at two different temperatures. *Anal. Chim. Acta* **2012**, *723*, 45−53.

https://doi.org/10.1021/acsomega.4c11143
ACS Omega 2025, 10, 11312−11324

(51) Zhang, J.; Hao, Y.; Tian, X.; Liang, Y.; He, X.; Gao, R.; Chen, L.; Zhang, Y. Multi-stimuli responsive molecularly imprinted nanoparticles with tailorable affinity for modulated specific recognition of human serum albumin. *J. Mater. Chem. B* **2022**, *10*, 6634−6643.
(52) Musarurwa, H.; Tawanda Tavengwa, N. Stimuli-responsive molecularly imprinted polymers as adsorbents of analytes in complex matrices. *Microchem. J.* **2022**, *181*, 107750.

https://doi.org/10.1021/acsomega.4c11143
ACS Omega 2025, 10, 11312−11324